Journal of Materials Chemistry C

ROYAL SOCIETY OF CHEMISTRY

PAPER

View Article Online
View Journal | View Issue

Cite this: J. Mater. Chem. C, 2024, 12, 11394

Fabrication of efficient and red-emissive salicylaldehyde Schiff base isomers for multi-scenario information decryption†

Weiren Zhong,‡[ab] Yanchen Wu,‡[a] Yuting Lin,[a] Shouji Li,[ab] Jianyu Zhang*[c] and Xu-Min Cai *[ab]

Received 30th March 2024,
Accepted 12th June 2024

DOI: 10.1039/d4tc01287a

rsc.li/materials-c

Due to their broad applications in information technology, biochemical sensors, and optoelectronic devices, stimuli-responsive fluorescent materials (SRFMs) have gained significant attention. With their simple synthesis and modification, Schiff bases are considered promising candidates for SRFMs. However, realizing highly efficient luminescence with aggregation-induced emission (AIE) properties as well as stimuli responses is still challenging due to the lack of clear structure–property relationships. In this work, a general strategy for constructing efficient and red-emissive salicylaldehyde Schiff bases is proposed utilizing the triphenylamine (TPA) substitution strategy. Experimental results and theoretical calculations illustrate that all four isomers show a typical AIE effect of the keto-form emission upon photoexcitation and red fluorescence due to the charge-transfer transition from TPA on the salicylaldehyde unit to the keto unit. The single-crystal structure also demonstrates that the introduction of dual TPA leads to appropriate intermolecular interactions, resulting in high-intensity fluorescence. Moreover, with excellent acidochromic properties under both daylight and UV light conditions, *p,p*-2TPA is successfully applied in steganography and multi-scenario information decryption. This work not only realizes efficient and red-colored luminescence from a simple salicylaldehyde Schiff base skeleton but also provides a strategy for constructing SRFMs with AIE properties.

Introduction

Stimuli-responsive fluorescent materials (SRFMs) are smart materials that can alter fluorescence signals in response to external stimuli, including light,[1,2] mechanical force,[3–5] temperature,[6,7] and pH.[8–10] Due to their vast potential applications in anti-counterfeiting,[11,12] information encryption–decryption,[13,14] biochemical sensors,[15–18] and optoelectronic devices,[19,20] the development of SRFMs has gained significant attention in recent years.[21] Hence, many conventional stimuli-responsive molecular scaffolds, such as spiropyran,[22,23] azobenzenes,[24,25] dihydroazulenes,[26,27] diarylethenes,[28,29] and Schiff bases,[30,31] have been developed with dynamic covalent bonds for advanced applications. For example, the stimuli-responsive properties of Schiff bases are derived from the isomerization of the central C=N double bonds and protonation processes of the nitrogen atom.[32] On the other hand, luminogens with aggregation-induced

[a] Jiangsu Co-Innovation Center of Efficient Processing and Utilization of Forest Resources, College of Chemical Engineering, Nanjing Forestry University, Nanjing 210037, China. E-mail: xumin.cai@njfu.edu.cn
[b] Guangdong Provincial Key Laboratory of Luminescence from Molecular Aggregates, Guangzhou 510640, China
[c] Stratingh Institute for Chemistry, University of Groningen, Nijenborgh 4, Groningen 9747 AG, The Netherlands. E-mail: jianyu.zhang@rug.nl

† Electronic supplementary information (ESI) available. CCDC 2343783. For ESI and crystallographic data in CIF or other electronic format, see DOI: https://doi.org/10.1039/d4tc01287a

‡ W. Zhong and Y. Wu contributed equally to this work.

Xu-Min Cai

Dr. Xu-Min Cai is an associate professor at Nanjing Forestry University (NJFU). She received her master's and PhD degrees from Nanjing University and Technical University of Munich, respectively. Afterwards, she joined NJFU at the College of Chemical Engineering in 2016, initiating multidisciplinary research on biomass-based aggregation-induced emission materials. She has published several representative papers in Nat. Commun., Natl. Sci. Rev., Adv. Sci., Aggregate, Chem. Sci., etc., with some promoted by news presses like AurekAlert and National Science Review. She is a young editorial board member for The Innovation and Biomass Chemical Engineering.

emission (AIE) properties, which are non-emissive in the solution state but can emit bright luminescence in the aggregate state, have recently paved the way for organic luminescent materials.[33,34] However, most molecules with AIE properties are constructed from triphenylamine (TPA) and tetraphenylethylene scaffolds, which do not show any stimuli-responsive behavior.[35,36] Therefore, designing luminogens with both AIE and stimuli-responsive properties is still challenging due to the limited molecular skeletons and unclear structure–property relationship. Nevertheless, one straightforward strategy is to combine the functional elements of these dynamic molecular scaffolds with AIE. With the advantages of simple synthesis, modification, and multifunctionality, Schiff base derivatives have great potential for constructing stimuli-responsive AIE materials and illustrating the underlying working mechanisms.

In previous works, single TPA and bromine groups were utilized to construct stimuli-responsive Schiff base derivatives.[2,37] However, these molecules exhibit two main issues: short emission wavelength and low fluorescence efficiency (Fig. 1a). The former can be attributed to the limited electronic conjugation, while the latter is ascribed to either too loose or overly tight aggregation. Loose aggregation reflects fewer intermolecular interactions, leading to active molecular motions and geometric relaxation in the excited state. In contrast, tight aggregation always leads to continuous intermolecular π–π stacking, resulting in long-range exciton diffusion and non-radiative decay.[38] Hence, it is believed that the substituents of the Schiff base skeleton play an essential role in regulating the aggregate structure and photophysical performance. To optimize the macroscopic performance, we envision grafting multiple TPA units onto the salicylaldehyde Schiff base scaffold. The broad conjugation effect of TPA can red-shift the emission wavelength, and the propeller-like structure can facilitate more intermolecular interactions and disrupt strong π–π stacking, finally increasing the luminescence efficiency.[39,40] Additionally, the salicylaldehyde Schiff base can undergo an excited-state intramolecular proton transfer (ESIPT) process between the imine and hydroxyl groups, resulting in the keto form in the excited state.[41] Therefore, the carbonyl group can serve as an electron acceptor, promoting the charge-transfer (CT) effect and red-shifting emission. Thus, introducing multiple TPA units is believed to be a strategy for constructing red-emission luminogens with high quantum yields (QYs).

In this work, we successfully synthesized four isomers with red emission by grafting two TPA units onto the salicylaldehyde Schiff base scaffold (Fig. 1b). The solvent effect reveals that the emission wavelength of the isomers red-shifts with increasing solvent polarity, indicating the presence of CT transition. The theoretical calculations also verify that the TPA substituent in the salicylaldehyde unit effectively affects the CT effect. Besides, single-crystal analysis demonstrates that *o*,*p*-2TPA exhibits appropriate intermolecular forces and lacks strong π–π stacking, resulting in high-intensity fluorescence. Furthermore, *p*,*p*-2TPA, with the highest quantum yield and red emission, displays excellent acidochromic luminescence (ACL) properties, endowing it with potential applications for information security protection. Accordingly, several examples of steganography and multi-scenario information decryption have been successfully applied as a proof-of-concept. This work provides a new strategy for developing high-intensity and red-emission AIE materials with stimuli-responsive properties based on salicylaldehyde Schiff bases.

Results and discussion

Synthesis and characterization

The synthesis routes to *o*,*p*-2TPA, *p*,*p*-2TPA, *o*,*o*-2TPA, and *p*,*o*-2TPA are depicted in Scheme 1. The detailed synthetic

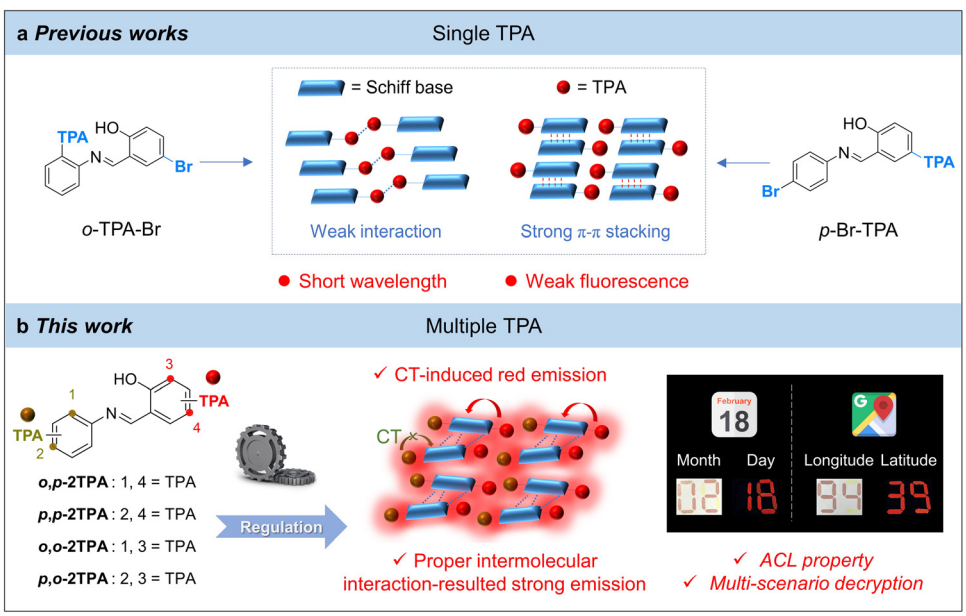

Fig. 1 (a) The structures and packing modes of salicylaldehyde Schiff bases modified by a single TPA unit. (b) Molecular design and properties of multiple-TPA modifications in this work.

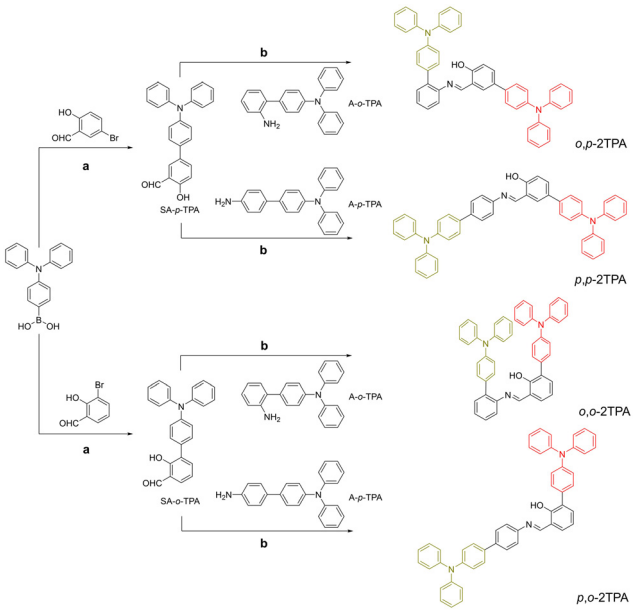

Scheme 1 Synthesis routes of *o*,*p*-2TPA, *p*,*p*-2TPA, *o*,*o*-2TPA, and *p*,*o*-2TPA: (a) toluene, K_2CO_3, $Pd(PPh_3)_4$, 115 °C, 6 h; and (b) EtOH, reflux, 80 °C, 3 h.

procedures are provided in the Experimental section of the ESI.† The structures and purity of these compounds are confirmed by ^{1}H NMR, ^{13}C NMR, HRMS, and single-crystal X-ray diffraction techniques (Fig. S1–S12 and Table S1, ESI†).

Aggregation-induced emission properties

First, the photophysical properties of these four compounds were investigated. Their absorption properties were similar, with the main absorption peaks at 310 nm and another shoulder peak corresponding to the CT transition at 374 nm (Fig. 2a).[42] Furthermore, their photoluminescence (PL) properties were examined in a mixed solvent system of tetrahydrofuran (THF) as the good solvent and water as the poor solvent. The fluorescence photographs show that they are almost non-emissive in mixtures with low water fractions (f_w) but are significantly emissive at high f_w, demonstrating the typical AIE property (Fig. 2). However, the four isomers show different emission curves. For example, *o*,*p*-2TPA, *p*,*p*-2TPA, and *o*,*o*-2TPA exhibit distinct dual-emission properties due to the ESIPT process (Fig. 2b–d). The short-wavelength and long-wavelength peaks are attributed to enol-form and keto-form emissions, respectively. In contrast, *p*,*o*-2TPA mainly exhibits long-wavelength emission from the keto form, indicating an efficient ESIPT process in the excited state upon photoexcitation (Fig. 2e). Although the changing trend of the enol-form emission is irregular, the emission intensity of the keto-form emission displays a typical AIE property. Accordingly, the relative emission intensity (α_{AIE}) of the keto form in mixtures with different f_w values was further plotted (Fig. 2f). With an increase in f_w within 0–50%, the intensity enhancement is negligible due to the flexible skeleton and active intramolecular motions before aggregation. When f_w increases to more than 60%, the intensities of all four isomers significantly increase, indicating the formation of aggregates and AIE characteristics. Furthermore, concentration-dependent and low-temperature experiments further confirm their AIE properties. With increasing concentration, the molecules tend to form aggregates and exhibit enhanced PL intensity (Fig. S13, ESI†). Similarly, fluorescence at 77 K is significantly enhanced compared to that under room temperature conditions (Fig. S14, ESI†), which supports the mechanism of restriction of intramolecular motions.[43,44] Therefore, the above results demonstrate the typical AIE properties of these salicylaldehyde Schiff bases with multiple TPA substituents.

Charge-transfer properties

The appearance of CT peaks in the absorption spectra indicates that these isomers exhibit certain CT properties (Fig. 2a), which may be attributed to the D–A structure formed due to the electron-donating properties of TPA units and the electron-withdrawing ability of the salicylaldehyde Schiff base.[45] To further investigate their CT effects, solvent-dependent PL spectra of these four isomers were obtained. Their absorption spectra show similar characteristics, with a slight red-shift within 350–400 nm in different solvents (Fig. S15, ESI†). Density functional theory (DFT) calculations based on the enol-form structure also indicate almost the same energy gaps between the highest occupied molecular orbital (HOMO) and the lowest unoccupied molecular orbital (LUMO) (Fig. S16, ESI†). However, the PL spectra in different polar solvents show obvious differences (Fig. 3). With increased polarity, the maximum emission wavelength of *o*,*p*-2TPA shifts from 606 nm in cyclohexane to 656 nm in dimethyl sulfoxide, exhibiting a red-shift of 50 nm. Meanwhile, *p*,*p*-2TPA shifts from 599 nm to 625 nm, showing a red-shift of 26 nm; *o*,*o*-2TPA shifts from 606 nm to 629 nm in *N*,*N*-dimethylformamide with a red-shift of 23 nm; and *p*,*o*-2TPA shifts from 617 nm to 631 nm in acetonitrile solvent with a red-shift of 14 nm. The above solvent effects clearly indicate the CT feature of the keto form.[46] DFT calculations were also carried out based on the optimized excited-state geometry as the keto form to evaluate the electron distribution. As shown in Fig. 3e, all isomers show the HOMO distribution on the TPA-modified salicylaldehyde unit. The electron of the LUMO is located in the salicylaldehyde part. However, only a few electrons are located on the TPA-substituted aniline part, suggesting that the CT effect mainly depends on the modification of the salicylaldehyde group. This result is consistent with a previous report.[37] In summary, the synergistic effect of the large Stokes shift caused by the ESIPT process and the CT transition in the keto form resulted in red emission from these isomers.

Solid-state properties

The photophysical properties of the four isomers in the solid state were further explored, which are crucial for practical applications. The UV-DRS spectra of the solid samples show a redshifted absorption wavelength compared to that in the solution state, indicating comparatively strong intermolecular interactions (Fig. S17, ESI†). The PL spectra show that the fluorescence wavelength is around 600 nm, reaching the red-colored region (Fig. 4a). This result suggests the universality of constructing red-light salicylaldehyde Schiff bases using the

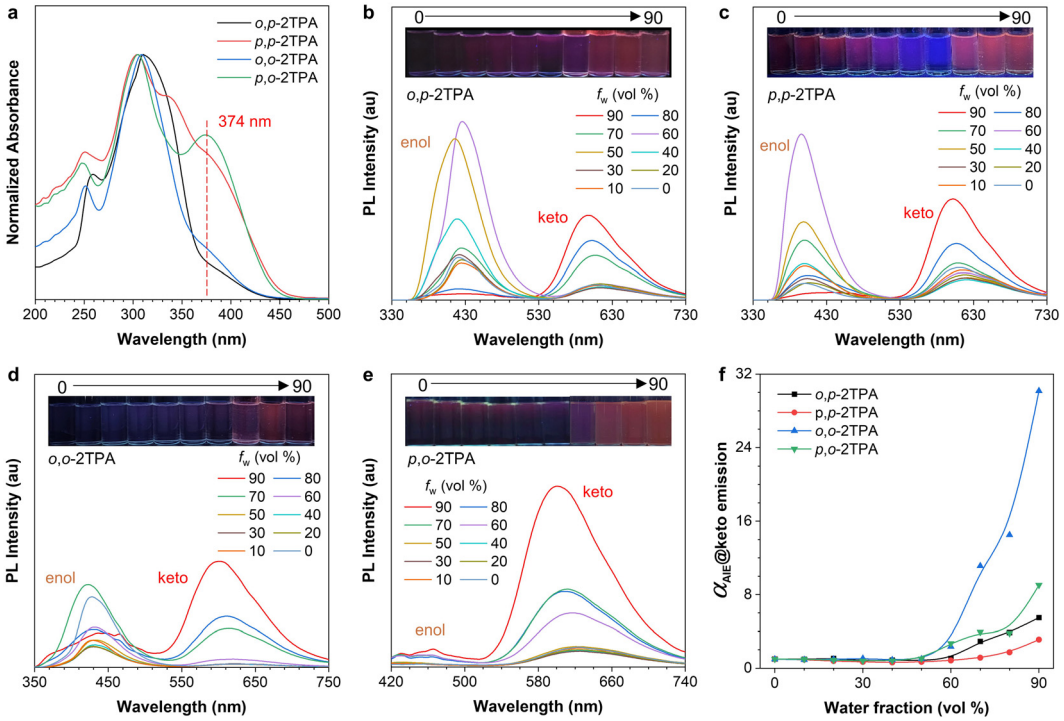

Fig. 2 (a) Normalized absorption spectra of the four isomers. (b)–(e) PL spectra of (b) *o*,*p*-2TPA, (c) *p*,*p*-2TPA, (d) *o*,*o*-2TPA, and (e) *p*,*o*-2TPA in THF/H_2O mixtures with different f_w values. λ_{ex} = 310 nm for *o*,*p*-2TPA, 304 nm for *p*,*p*-2TPA, 308 nm for *o*,*o*-2TPA, and 374 nm for *p*,*o*-2TPA. Inset: fluorescence photographs taken under 365 nm UV irradiation. Concentration: 20 μM. (f) Plots of relative keto-form emission intensity ($\alpha_{AIE} = I/I_0$) *versus* different f_w values of the four isomers. I_0 = PL intensity in pure THF solution.

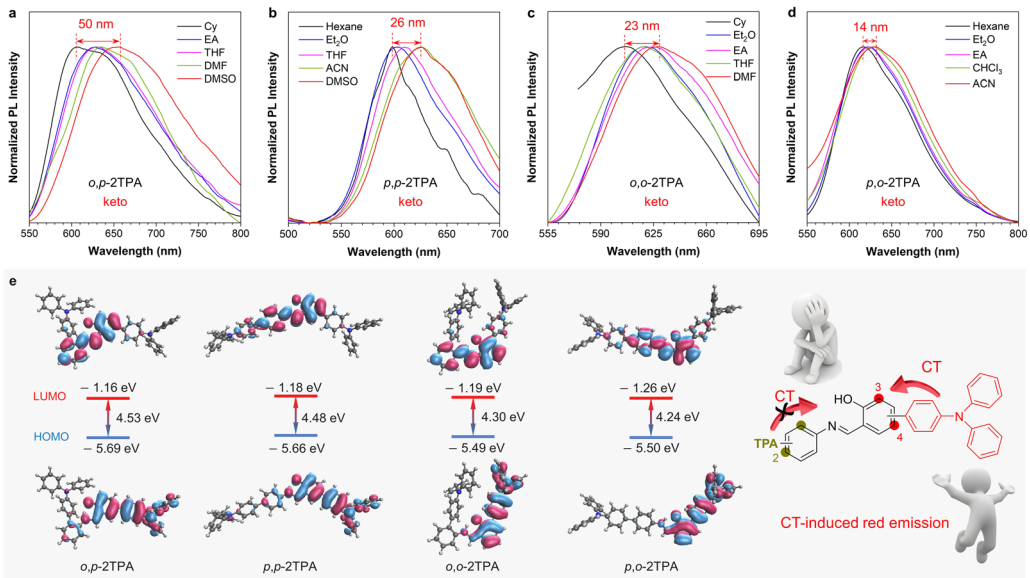

Fig. 3 Normalized PL spectra of (a) *o*,*p*-2TPA, (b) *p*,*p*-2TPA, (c) *o*,*o*-2TPA, and (d) *p*,*o*-2TPA in different solvents with varying polarities. (e) Frontier molecular orbitals of the four isomers and the energy gaps between the HOMO and LUMO.

dual-TPA strategy. However, *o*,*o*-2TPA and *p*,*o*-2TPA are weakly emissive with absolute QYs of 0.59% and 0.83%, respectively (Fig. 4b). In contrast, *o*,*p*-2TPA and *p*,*p*-2TPA show comparatively high efficiency with absolute QYs of 11.15% and 14.52%, respectively, which are much higher than those of the mono-TPA-substituted compounds (*o*-TPA-Br: 0.6% and *p*-Br-TPA: 0%), as reported in previous work.[2,37] The above results also indicate that the *para*-substituted position of the phenol group in the salicylaldehyde Schiff base scaffold is more conducive than the *ortho*-substituted position to produce efficient luminescence.

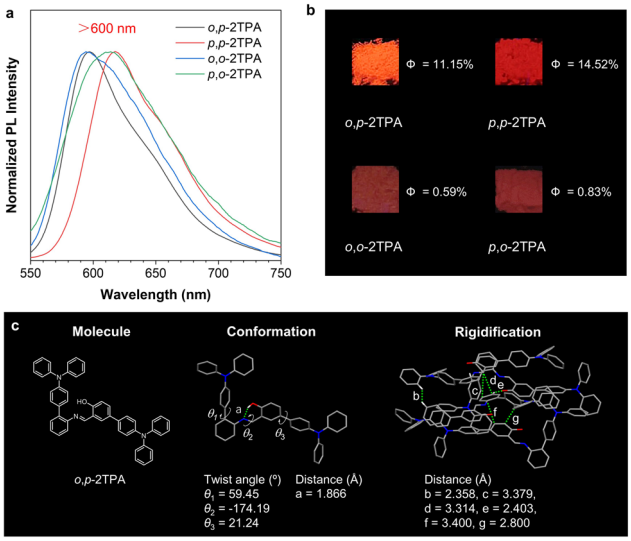

Fig. 4 (a) Normalized PL spectra of the four isomers as solids. λ_{ex} = 429 nm for *o,p*-2TPA, 476 nm for *p,p*-2TPA, 405 nm for *o,o*-2TPA, and 466 nm for *p,o*-2TPA. (b) Fluorescence photographs and quantum yields of the four isomers. (c) Chemical structure, twist conformation, and intermolecular interactions based on the single-crystal structure of *o,p*-2TPA.

Fortunately, single crystals of *o,p*-2TPA were obtained by slow evaporation of its EtOH/DCM (2 : 1, *v*/*v*) solution (Fig. 4c and Table S1, ESI†), which may provide more insight into its high efficiency with red luminescence. From the single-crystal structure resolved *via* the X-ray diffraction technique, the torsion angles of the two TPA units around the core are 59.45° and 21.24°, respectively, indicating that the twisted conformation of *o,p*-2TPA limits π–π stacking to prevent fluorescence quenching. The packing arrangement suggests multiple intermolecular interactions with appropriate distances of 2.358–3.400 Å, which is beneficial to provide a solidification environment to suppress non-radiative decay. In comparison, the intermolecular interactions of *o*-TPA-Br are mainly H···H interactions, and the packing of *p*-Br-TPA is denser.[2,37] The above analysis clearly supports the modification strategy with multiple TPA units to provide the appropriate packing mode and transition characteristics of luminogens in the solid state and finally endow them with red emission and high QY.

Encryption and decryption enabled by ACL

Usually, a Schiff base scaffold with an imine bond exhibits ACL properties, which can undergo acid/base-stimuli responses (Fig. S18, ESI†). With the highest QY and red emission, *p,p*-2TPA was chosen as an example to investigate the ACL performance. As shown in Fig. 5a, pristine *p,p*-2TPA exhibits an emission peak at 600–650 nm. The emission peak disappears after exposure to trifluoroacetic acid (TFA) vapor, indicating fluorescence quenching. Subsequent exposure to triethylamine (TEA) vapor results in the reappearance of the emission peak. To explore the mechanism behind this observation, the ^{1}H NMR spectra of the sample before and after TFA treatment were measured (Fig. 5b). When excess TFA was added to the $CDCl_3$ solution, the hydrogen signal of the –N=CH– unit shifted to a lower field, demonstrating protonation of *p,p*-2TPA under acidic conditions.[47] As shown in Fig. S19 (ESI†), the fluorescence spectra of the solution and solid samples indicate that the emission peak of the enol form increases in proportion after acid treatment. Hence, the protonated imine group blocks the ESIPT process, which finally quenches the long-wavelength fluorescence from the keto form.[48] After TEA fuming, the hydrogen signal of the –N=CH– unit returns to the high field, and the keto peak increases (Fig. 5b and Fig. S19, ESI†), indicating deprotonation and reactivation of the ESIPT process (Fig. 5c). As a result, red fluorescence was recovered. By leveraging the characteristics of fluorescence quenching and activation under acid/base stimuli, *p,p*-2TPA can be used for information steganography. As shown in Fig. 5d, *p,p*-2TPA solution was utilized as the ink to write the letter "E" on a paper, which appears under UV irradiation. When exposed to

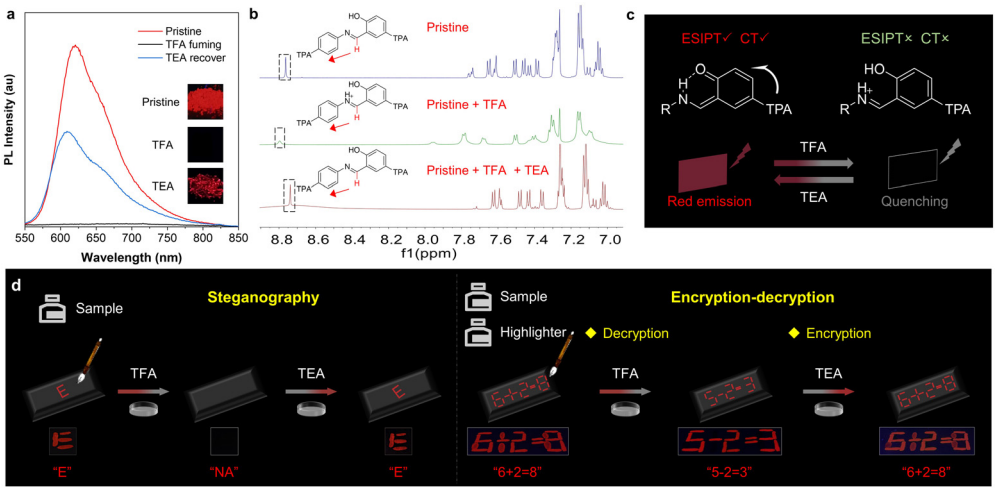

Fig. 5 (a) PL spectra of solid *p,p*-2TPA after different treatments. Inset: fluorescence photographs taken after the different treatments. (b) ^{1}H NMR spectra of *p,p*-2TPA before and after the addition of TFA and TEA in $CDCl_3$. (c) Schematic diagram of the luminescence mechanism behind acid/base stimuli. (d) Application of stimuli-responsive *p,p*-2TPA for steganography and information encryption and decryption.

TFA vapor, the letter "E" disappears with fluorescence quenching, resulting in hidden information. After subsequent exposure to TEA, the letter "E" reappears due to the reactivation of the ESIPT process. To further demonstrate its potential application in information encryption and decryption, *p*,*p*-2TPA was combined with commercial fluorescent dyes of the same color to achieve more concealed information transmission. Since these commercial fluorescent dyes do not exhibit ACL properties, dynamic information can be observed under different stimuli. For instance, the information of "6 + 2 = 8" is written on a paper using *p*,*p*-2TPA and commercial fluorescent dyes, which could be observed under UV irradiation. However, after exposure to TFA vapor, only emissive signals from the commercial dye display the decrypted information of "5 − 2 = 3". After exposure to the TEA vapor, the encrypted information of "6 + 2 = 8" is restored to its original state. Therefore, by controlling the external stimuli of the acid and base, a sensitive fluorescence signal from *p*,*p*-2TPA can be applied in steganography and information encryption–decryption.

Interestingly, apart from fluorescence, the absorption of *p*,*p*-2TPA responds to external acid/base stimuli. The UV-DRS spectra exhibit an absorption peak at around 700 nm upon exposure in TFA.[49] Subsequent TEA treatment could not significantly reduce the intensity of the peak due to incomplete deprotonation and residual protonated product in the solid state (Fig. S20, ESI†). Therefore, it is possible to realize complicated information encryption and decryption by synergistically utilizing the responsive changes in absorption and fluorescence. Therefore, a schematic diagram depicting the application of *p*,*p*-2TPA stimulated by TFA and TEA is proposed (Fig. 6a). Initially, when the *p*,*p*-2TPA solution is used as an ink to write, there is no obvious color present under daylight, making it impossible to obtain information. As a comparison, its fluorescent signal is very intense, revealing a clear message of "A". After TFA fuming, the absorption is deepened with the clear letter "A", but its fluorescence is quenched, and it is unable to display information. Further, the sample's absorption can still be observed upon TEA fuming, showing the message of "A". Hence, the above phenomenon demonstrates that different information can be obtained through the absorption and fluorescence signals of *p*,*p*-2TPA, respectively, achieving complex information encryption and decryption. Accordingly, some demonstrations using *p*,*p*-2TPA and commercial dyes were developed as proof-of-concept.[2] As shown in Fig. 6b, information "A" is written using a commercial dye with red fluorescence, information "I" is written with non-fluorescent commercial dye, and information "E" is written with *p*,*p*-2TPA. First, the presentation of "AI" under daylight and "AE" under UV light is achieved. After TFA fuming, the complete information of "AIE" displays under daylight, but only "A" shows as the fluorescence signal. Finally, upon TEA fuming, these two signals become "AIE" and "AE", respectively. Using the same approach, multi-scenario information decryption was developed (Fig. 6c). The information of "02 18" representing the date of " February 18th" is initially obtained using a combination of absorption and fluorescence signals. After TFA and TEA fuming, the data "August 12th" and "August 18th" can be interpreted. Similarly, it is possible to switch the information between "94 39", "99 34", and "99 39". These data can be input into the corresponding mobile positioning program, and the specific locations can be determined as "94°E, 39°N", "99°E, 34°N", and "99°E, 39°N", respectively. The above results support the potential application of these compounds with ACL properties for multi-scenario information encryption and decryption through different sensitivities of absorption and fluorescence.

Conclusions

In summary, four isomers (*o*,*p*-2TPA, *p*,*p*-2TPA, *o*,*o*-2TPA, and *p*,*o*-2TPA) were synthesized by introducing two TPA units into the salicylaldehyde Schiff base scaffold. Photophysical and solvent effect experiments demonstrate that all four compounds exhibit typical AIE properties, ESIPT upon photoexcitation, and CT characteristics. DFT calculations have revealed that the TPA substituent on the salicylaldehyde moiety plays a predominant role in the CT effect, which results in long-wavelength emission with a red color. Single-crystal analysis reveals that the incorporation of dual TPA moieties introduces

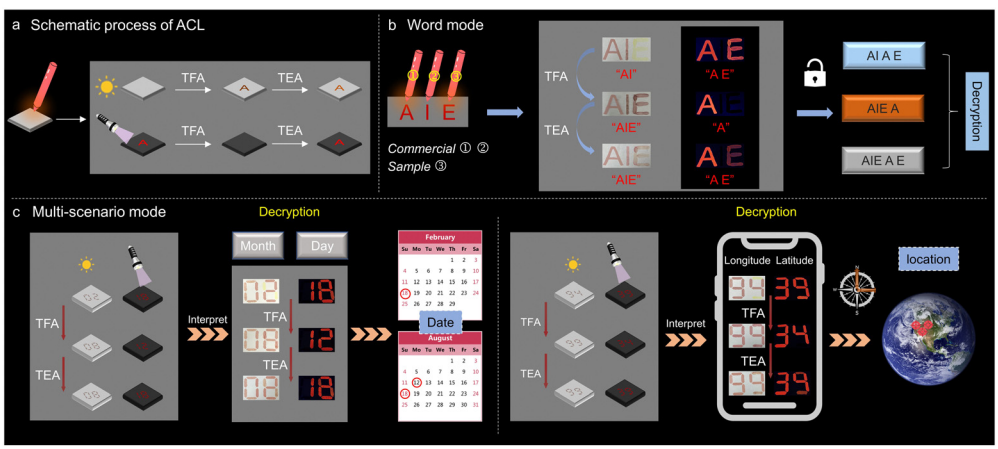

Fig. 6 (a) Schematic process of ACL. (b) and (c) Practical information decryption of the word and multi-scenario modes.

appropriate intermolecular interactions, which prevent strong π–π stacking and effectively restrict intramolecular motions, promoting highly efficient fluorescence. More significantly, *p*,*p*-2TPA displays excellent ACL properties under acid/base stimuli. Therefore, several examples based on *p*,*p*-2TPA have been used to show multiple pieces of information, demonstrating successful applications in steganography and multi-scenario information decryption. This work provides a design strategy for dual TPA modification to realize the construction of efficient and red-emissive AIE materials with stimuli responses based on a salicylaldehyde Schiff base scaffold.

Author contributions

Weiren Zhong: validation, formal analysis, investigation, and writing – original draft. Yanchen Wu: formal analysis, investigation, and writing – original draft. Yuting Lin: investigation. Shouji Li: investigation. Jianyu Zhang: methodology, funding acquisition, supervision, validation, and writing – review & editing. Xu-Min Cai: conceptualization, methodology, formal analysis, resources, data curation, writing – review & editing, visualization, supervision, project administration, and funding acquisition.

Data availability

The authors confirm that the data supporting the findings of this study are available within the article and/or its ESI.†

Conflicts of interest

There are no conflicts to declare.

Acknowledgements

The authors are grateful to the National Natural Science Foundation of China (21601087), the Natural Science Foundation of Jiangsu Province (BK20231296), and the Open Fund of Guangdong Provincial Key Laboratory of Luminescence from Molecular Aggregates, Guangzhou 510640, China (South China University of Technology (2023B1212060003)). J. Zhang acknowledges the support from the Marie Skłodowska-Curie Actions grant under the Programme of Horizon Europe (101105790).

Notes and references

1 B. Shao, M. Baroncini, H. Qian, L. Bussotti, M. Di Donato, A. Credi and I. Aprahamian, *J. Am. Chem. Soc.*, 2018, **140**, 12323–12327.
2 X.-M. Cai, W. Zhong, Z. Deng, Y. Lin, Z. Tang, X. Zhang, J. Zhang, W. Wang, S. Huang, Z. Zhao and B. Z. Tang, *Chem. Eng. J.*, 2023, **466**, 143353.
3 Y. Sagara, M. Karman, E. Verde-Sesto, K. Matsuo, Y. Kim, N. Tamaoki and C. Weder, *J. Am. Chem. Soc.*, 2018, **140**, 1584–1587.
4 X.-M. Cai, Z. Tang, X. Chen, Y. Lin, X. Zhang and S. Huang, *Dyes Pigm.*, 2022, **204**, 110454.
5 J. Jiang, C. Hu, Y. Wang, L. Ma and J. Guo, *Mater. Today Chem.*, 2023, **30**, 101548.
6 Y.-H. Yang, Y.-S. Chen, W.-T. Chuang and J.-S. Yang, *J. Am. Chem. Soc.*, 2024, **146**, 8131–8141.
7 P. L. Jacquemin, K. Robeyns, M. Devillers and Y. Garcia, *Chem. Commun.*, 2014, **50**, 649–651.
8 Y. Xiong, W. Zhong, X. Zhang, Y. Lin, Z. Tang, S. Li and X.-M. Cai, *Dyes Pigm.*, 2023, **218**, 111475.
9 S. Ghosh, M. Avais and S. Chattopadhyay, *Chem. Commun.*, 2022, **58**, 12807–12810.
10 X. Li, R. Yue, G. Guan, C. Zhang, Y. Zhou and G. Song, *Exploration*, 2023, **3**, 20220002.
11 X. Yu, H. Zhang and J. Yu, *Aggregate*, 2021, **2**, 20–34.
12 Y. Shen, X. Le, Y. Wu and T. Chen, *Chem. Soc. Rev.*, 2024, **53**, 606–623.
13 L. X. Hou, H. Ding, X. P. Hao, C. N. Zhu, M. Du, Z. L. Wu and Q. Zheng, *Soft Matter*, 2022, **18**, 2149–2156.
14 C. Yang, H. Xiao, L. Tang, Z. Luo, Y. Luo, N. Zhou, E. Liang, G. Wang and J. Tang, *Mater. Horiz.*, 2023, **10**, 2496–2505.
15 L.-L. Chen, Z.-L. Wang, L. Sun, X.-B. Sun and W. Gu, *J. Photoch. Photobio. A*, 2023, **438**, 114533.
16 L. Sun, L. Chen, Z. Yang, X. Sun, D. Jin, Y. Qiu and W. Gu, *J. Food Compos. Anal.*, 2023, **120**, 105316.
17 L. Sun, M. Li, L. Chen, X. Sun, Z. Yang, S. Wang and W. Gu, *J. Lumin.*, 2023, **257**, 119658.
18 J. Tang, W. Lu, J. Hu, Y. Jia, X. He, L. Li, S. Yang, Y. Wang and L. Xu, *J. Mol. Struct.*, 2024, **1301**, 137448.
19 Y. Xia, Y. Zhu, B. Yang, W. Guo, S. Han and X. Wang, *Nano Energy*, 2022, **102**, 107653.
20 H. Al-Kutubi, H. R. Zafarani, L. Rassaei and K. Mathwig, *Eur. Polym. J.*, 2016, **83**, 478–498.
21 G. Shi and D. Xue, *Prog. Nat. Sci: Mater. Int.*, 2022, **32**, 674–683.
22 J. Sheng, J. Perego, S. Bracco, W. Czepa, W. Danowski, S. Krause, P. Sozzani, A. Ciesielski, A. Comotti and B. L. Feringa, *Adv. Mater.*, 2024, **36**, 2305783.
23 J. Xie, J. Zhang, Y. Ma, Y. Han, J. Li and M. Zhu, *J. Mater. Chem. C*, 2022, **10**, 7154–7166.
24 E. Fuentes, M. Gerth, J. A. Berrocal, C. Matera, P. Gorostiza, I. K. Voets, S. Pujals and L. Albertazzi, *J. Am. Chem. Soc.*, 2020, **142**, 10069–10078.
25 S. Wang, P. Poudel, F. H. Schacher and L. I. Kaberov, *Polym. Chem.*, 2023, **14**, 3381–3391.
26 J. Zhang, H. Shen, X. Liu, X. Yang, S. L. Broman, H. Wang, Q. Li, J. W. Y. Lam, H. Zhang, M. Cacciarini, M. B. Nielsen and B. Z. Tang, *Angew. Chem., Int. Ed.*, 2022, **61**, e202208460.
27 H. Torres-Pierna, C. Roscini, A. Vlasceanu, S. L. Broman, M. Jevric, M. Cacciarini and M. B. Nielsen, *Dyes Pigm.*, 2017, **145**, 359–364.
28 M. Morant-Giner, J. M. Carbonell-Vilar, M. Viciano-Chumillas, A. Forment-Aliaga, J. Cano and E. Coronado, *J. Mater. Chem. C*, 2021, **9**, 10975–10984.
29 I. C.-Y. Hou, F. Berger, A. Narita, K. Müllen and S. Hecht, *Angew. Chem., Int. Ed.*, 2020, **59**, 18532–18536.

30 H. Sun, S.-S. Sun, F.-F. Han, Y. Zhao, M.-D. Li, B.-X. Miao, J. Nie, R. Zhang and Z.-H. Ni, *Chem. Eng. J.*, 2021, **405**, 127000.
31 X.-H. Ding, L.-Z. Wang, Y.-Z. Chang, C.-X. Wei, J.-Y. Lin, M.-H. Ding and W. Huang, *Aggregate*, 2024, **5**, e500.
32 A. Huang, J. Hu, M. Han, K. Wang, J. L. Xia, J. Song, X. Fu, K. Chang, X. Deng, S. Liu, Q. Li and Z. Li, *Adv. Mater.*, 2021, **33**, 2005249.
33 L. Biesen and T. J. J. Müller, *Aggregate*, 2021, **2**, e105.
34 J. Yang, M. Fang and Z. Li, *Aggregate*, 2020, **1**, 6–18.
35 H.-J. Yen, C.-J. Chen and G.-S. Liou, *Chem. Commun.*, 2013, **49**, 630–632.
36 T. Fumoto, R. Tanaka and Y. Ooyama, *Dalton Trans.*, 2023, **52**, 5047–5055.
37 W. Zhong, J. Zhang, Y. Lin, S. Li, Y. Yang, W.-J. Wang, C. Si, F. E. Kühn, Z. Zhao, X.-M. Cai and B. Z. Tang, *Chem. Sci.*, 2024, **15**, 3920.
38 Y. Gu, Z. Zhao, H. Su, P. Zhang, J. Liu, G. Niu, S. Li, Z. Wang, R. T. K. Kwok, X.-L. Ni, J. Sun, A. Qin, J. W. Y. Lam and B. Z. Tang, *Chem. Sci.*, 2018, **9**, 6497–6502.
39 Y. Yang, J. Wang, D. Li, J. Yang, M. Fang and Z. Li, *Adv. Mater.*, 2021, **33**, e2104002.
40 B. He, J. Huang, J. Zhang, H. H. Y. Sung, J. W. Y. Lam, Z. Zhang, S. Yan, D. Wang, J. Zhang and B. Z. Tang, *Angew. Chem., Int. Ed.*, 2022, **61**, e202117709.
41 P. Zhou and K. Han, *Aggregate*, 2022, **3**, e160.
42 D. Pinjari, A. Z. Alsaleh, Y. Patil, R. Misra and F. D'Souza, *Angew. Chem., Int. Ed.*, 2020, **59**, 23697–23705.
43 J. Zhang, H. Zhang, J. W. Y. Lam and B. Z. Tang, *Chem. Res. Chin. Univ.*, 2021, **37**, 1–15.
44 X.-M. Cai, Y. Lin, Y. Li, X. Chen, Z. Wang, X. Zhao, S. Huang, Z. Zhao and B. Z. Tang, *Nat. Commun.*, 2021, **12**, 1773.
45 J. Zhang, Y. Tu, H. Shen, J. W. Y. Lam, J. Sun, H. Zhang and B. Z. Tang, *Nat. Commun.*, 2023, **14**, 3772.
46 X.-M. Cai, S. Li, W. J. Wang, Y. Lin, W. Zhong, Y. Yang, F. E. Kühn, Y. Li, Z. Zhao and B. Z. Tang, *Adv. Sci.*, 2024, **11**, 2307078.
47 P. Xue, P. Chen, J. Jia, Q. Xu, J. Sun, B. Yao, Z. Zhang and R. Lu, *Chem. Commun.*, 2014, **50**, 2569–2571.
48 R. Plaza-Pedroche, M. P. Fernández-Liencres, S. B. Jiménez-Pulido, N. A. Illán-Cabeza, S. Achelle, A. Navarro and J. Rodríguez-López, *ACS Appl. Mater. Inter.*, 2022, **14**, 24964–24979.
49 T. Ma, S. Chen, X. Du, M. Mo and X. Cheng, *Dyes Pigm.*, 2023, **213**, 111176.